POLITECNICO
MILANO 1863

SCUOLA DI INGEGNERIA INDUSTRIALE
E DELL'INFORMAZIONE

Executive Summary of the Thesis

Performance analysis and simulations of a laboratory X-ray Absorption Spectrometer

Laurea Magistrale in Physics Engineering - Ingegneria Fisica

Author: Piero Florio

Advisor: Prof. Marco Moretti

Co-advisor: Prof. Giacomo Ghiringhelli

Academic year: 2021-2022

1. Introduction

X-ray Absorption Spectroscopy (XAS) is a well established non destructive method for determining both the oxidation state and the local environment of a given element in a material [1]. In X-ray Absorption Spectroscopy (XAS) a core-electron is promoted into an empty electronic state above the Fermi level by absorption of an X-ray and, as such, XAS probes the unoccupied density of states. The Near-Edge (XANES) region of the spectrum is mostly sensitive to the oxidation state of the absorber and to the geometrical coordination of the ligands, while the Extended region provides information on the Fine Structure (EXAFS), i.e., the interatomic distances of the first few coordination shells around the absorber in both crystalline and amorphous materials. Very informative are XANES and EXAFS measurements at the K-edges of 3d and L-edges of 5d transition metals, which lie in the $5 - 15$ keV energy range. The flexibility of the technique allows the analysis of samples of different nature (from solids to liquid and gases) and can find applications in various fields, finding fertile ground in basic physics and chemistry as well as in studies on cultural heritage. After the advent of synchrotron radiation sources, XAS experiments are mainly performed at synchrotron facilities because of the obvious advantages offered by their light. However, the limited access to synchrotron beamtime reduces and nearly excludes a large number of potentially important scientific researches to be performed. It is precisely for this reason that laboratory XAS spectrometers are considered, again generating interest within the scientific community, also thanks to the development of increasingly performing X-ray sources. In this contest, the XAS instrument being designed by the PoliMiX group is extremely welcome.

2. XAS in laboratory

The working principle of a XAS experiment is schematized in Figure 1. A polychromatic source emits a beam $I_0(E)$; each spectral component of the incoming beam is differently absorbed by a sample of thickness t giving rise to the transmitted radiation $I(E)$. Simply by comparison between $I(E)$ and $I_0(E)$ it is possible to find the absorption coefficient $\mu(E)$ of the sample:

$$\mu(E) = \frac{1}{t} \ln \frac{I_0(E)}{I(E)}$$

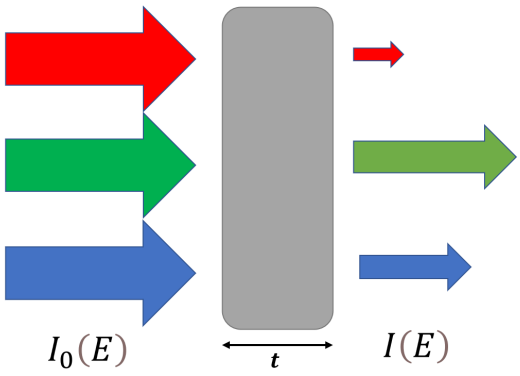

Figure 1: The spectral components of the incoming radiation I_0 are differently absorbed by a sample of thickness t due to the energy dependency of the absorption coefficient $\mu(E)$.

It is known as Lambert-Beer Law. It is clear how, in order to calculate this ratio, it is necessary to distinguish the different spectral components of the beam. To do that a crystal (analyzer) that exploits a Bragg reflection is used

$$E(\theta_B) = \frac{nhc}{2d \sin \theta_B} \tag{1}$$

where E is the energy selected by the monochromator, d is the distance between its crystallographic planes, n is an integer number representing the order of the reflected harmonic and θ_B is the angle that the polychromatic incident radiation forms with the analyzer surface. Finally, a detector is required to measure the intensity of the different spectral components.

2.1. The Rowland Setup

Source, crystal and detector must be properly placed in order to correctly work. In particular, we will focus our attention on the Rowland geometry setup that features a bent crystal analyzer which plays the double role of monochromatizing the incident radiation and focusing it on the detector [2]. We preferred the Rowland geometry to a dispersive setup because the use of an ideally point-like detector enhances the signal-to-noise ratio. The three elements must be positioned on a circumference [3] with diameter equal to the curvature radius R of the crystal (see Figure 2). Since the energy selected by the monochromator depends on the incidence angle θ_B of the radiation on the crystal, two of the three elements must be moved during an energy scan.

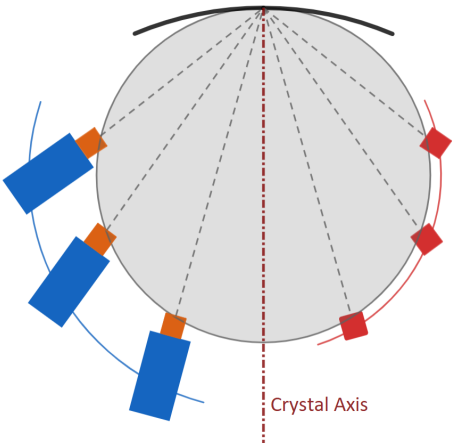

Figure 2: Schematic representation of a scan in energy: source (blue) and detector (red) must move specularly with respect to the axis of the crystal.

Within my thesis activity, I mostly focused on the characterization and optimization of the energy resolving properties of the instrument. In fact it is clear how the ability of the analyzer to monochromatize the radiation has a direct impact on the performances of the instrument. Unfortunately, it is not possible to perfectly monochromatize radiation for at least two reasons:

1. *Geometric aspects:* because of the extension of the crystal and of the source, the rays will not impinge the crystal at exactly the same angle θ_B causing a broadening of the reflected bandwidth that we will call *geometric contribution to energy resolution*;
2. *Intrinsic aspects:* a more complete treatment of diffraction (dynamic theory of diffraction) leads to modify equation 1 including the effects generated by multiplanar reflections and by the curvature of the crystal. These aspects are directly linked to a broadening of the reflected bandwidth that we will call *intrinsic contribution to energy resolution*;

As the name suggests, the last contribution cannot be avoided while, the *geometric contribution to energy resolution* can be drastically reduced optimizing the geometry of the instrument and choosing properly the crystal. For this reason, a large part of this thesis work is dedicated to the analytical and simulated study of the *geometric contribution to energy resolution.*

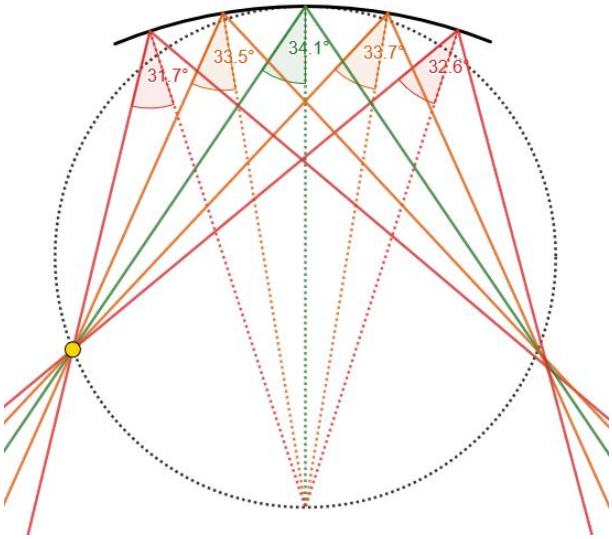

Figure 3: Geometric resolution worsening of a *Johann Crystal*. The Bragg angle is not exactly the same all over the surface of the crystal even for a point-like source.

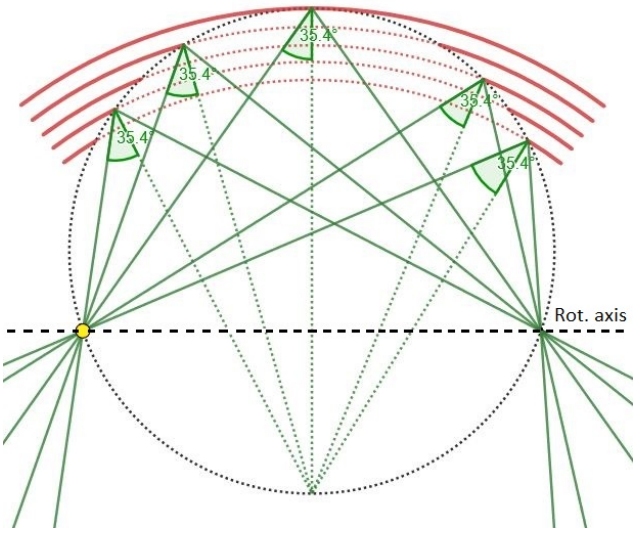

Figure 4: The crystallographic planes of a *Johansson crystal* are represented in red. In dashed red the portion of crystal to be removed starting from a Johann-type crystal. The graphical simulation undoubtedly shows how the incidence angles are equal over the entire surface of the crystal and how the radiation is focused exactly in one point.

3. Choice of the crystal

An appropriate choice of the crystal is certainly the first step to improve the energy resolution of the spectrometer. The most commonly used curved crystals are called *Johann-type* crystals and their monochromating properties are represented in Figure 3: as shown, a generic incidence angle away from the optical axis slightly differs from the central one (green). This inevitably leads to an unwanted worsening of the energy resolution that becomes more and more relevant as θ_B decreases. The origin of this effect lies in the fact that the reflections do not occur exactly on the Rowland circle (dashed circumference) but away from it. On the other hand, however, the fact that the curvature radius of the crystal is two times that of Rowland's circle is necessary as dictated by the equation of mirrors. The only way to overcome this problem is to shape the surface of the crystal in such a way that it fits in every point the Rowland's circle. The *Johansson-type* crystal thus obtained and represented in Figure 4 perfectly cancels Johann's aberrations. For this reason, despite the higher cost, we opted for this solution.
However, the reasoning made up to now is referred to the simplified two-dimensional case shown in Figure 4. Considering the ideal case in which source and detector are point-like it is clear that a rotational symmetry around the axis passing through them exists (see Figure 4). The ideal crystal surface will therefore be obtained simply by rotating the two-dimensional set-up around this axis. However, one thing is immediately evident: the position of the axis (more precisely its distance from the center of the analyzer) changes with Bragg angle. The ideal crystal should therefore have a *toroidal shape* in which the meridional radius is fixed and equal to the diameter of the Rowland circle while the sagittal radius must be dynamically changed during the scan. The first idea that might come to mind is to take a crystal with fixed meridional curvature R_m and change the sagittal one (R_s) by applying a variable torque to the analyzer during the scan. This procedure, however, is technically unfeasible. A more realistic approach is to approximate the ideal crystal surface by a set of independent cylindrical stripes of finite width whose relative positions can be dynamically adjusted as a function of Bragg angle (see Figure 5). All the following considerations will therefore refer to one of such stripes, i.e. to a cylindrical Johansson type crystal.

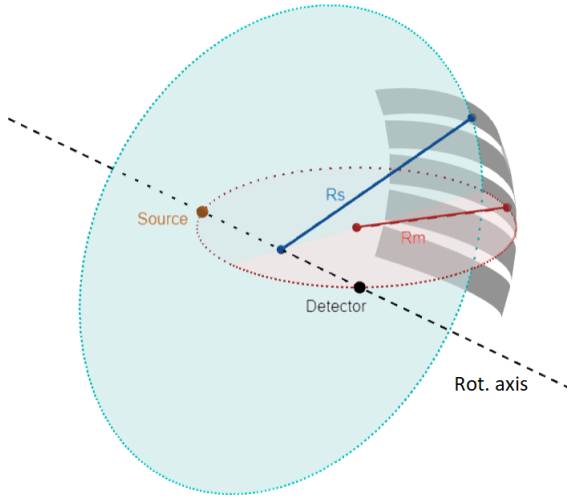

Figure 5: Five cylindrical stripes that approximate the ideal toroidal shape. While R_m (meridional radius) is fixed, R_s (sagittal radius) should be changed during the scan.

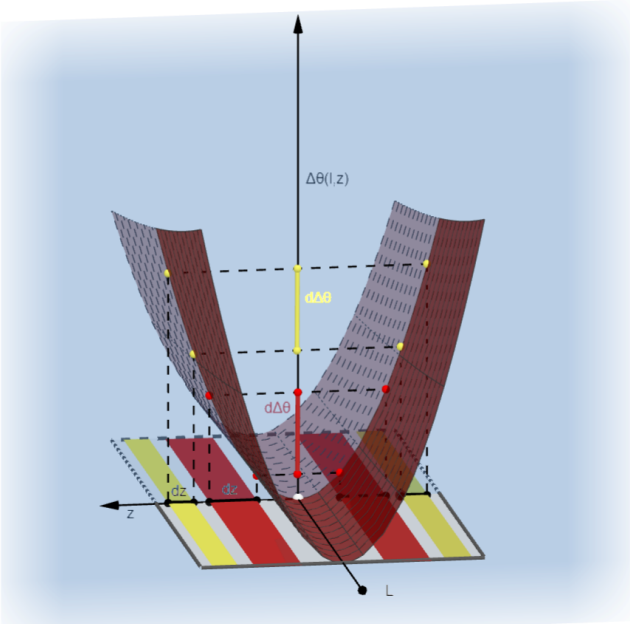

Figure 6: Graphical view of the probability $p_a(\Delta\theta_a)d\Delta\theta_a$ under the hypothesis of uniform irradiation of the analyzer. The probability, for a ray, to fall in the interval $d\Delta\theta_a$ red (yellow) is represented by the ratio between the two red (yellow) areas and the analyzer surface (gray). The probability decreases moving away from the center of the analyzer in the z direction.

4. Geometric contribution to energy resolution

Both the cylindrical analyzer and the finite size of the source will have an impact on the energy resolution of the spectrometer. An analytical approach will be followed by the results obtained by ray tracing simulations with the dual purpose of providing accurate results and validating the analytical calculations.

4.1. The analytical approach

In order to take into account only the analyzer contribution to the energy resolution, a point-like source is assumed to start with. The first result obtained is the relationship that expresses the deviation $\Delta\theta_a$ of the incidence angle with respect to the Bragg angle as a function of the length l and height z coordinates of the crystal:

$$\Delta\theta_a = \tan\theta_B \left(\frac{z^2}{2(R\sin\theta_B - l\cos(\theta_B - \frac{l}{R}))^2} \right) \tag{2}$$

This result is of particular interest since, unlike what is reported in literature [4], it also takes into account the effects caused by the length of the crystal. In order to estimate the average geometric contribution of the analyzer it is necessary to properly weight $\Delta\theta_a$ by its probability distribution, i.e. by the number of rays that hit the analyzer under that angular deviation. The probability distribution is easily found through geometric considerations and is reported below:

$$p_a(\Delta\theta_a) = \frac{R\sqrt{\sin\theta\cos\theta}}{\sqrt{2\Delta\theta_a}\cdot Z} \propto \frac{1}{\sqrt{\Delta\theta_a}} \tag{3}$$

Following exactly the same approach for the source contribution to energy resolution is possible to find

$$\Delta\theta_s \simeq -\frac{s_y}{R\sin\theta_B} \tag{4}$$

where s_y represents the meridional coordinate of a generic point of the source. An important result is that the sagittal coordinate s_z has a negligible impact on the resolution of the spectrometer. In analogy to what was done previously, it is possible to calculate the probability distribution associated to $\Delta\theta_s$, taking into account the fact that the intensity of the source has a Gaussian profile. The resulting probability distribution is also a Gaussian:

$$p_s(\Delta\theta_s) = C \cdot \exp\left[-\frac{R^2 \sin^2\theta_B (\Delta\theta_s)^2}{2\sigma_y^2}\right] \quad (5)$$

The last step to complete the theoretical treatment of the geometric contribution is to evaluate simultaneously the effects of the analyzer and of the source. It is demonstrated that the total angular deviation $\Delta\theta_g$ is given by:

$$\Delta\theta_g \simeq \Delta\theta_a + \Delta\theta_s$$

Since $\Delta\theta_a$ and $\Delta\theta_s$ are decoupled and independent, the overall probability distribution is obtained by convolving the probability distributions of $\Delta\theta_a$ and $\Delta\theta_s$, that is

$$p_g(\Delta\theta) = \int p_a(\Delta\theta - \Delta\theta') p_s(\Delta\theta') d\Delta\theta' \quad (6)$$

Our analytical results are then compared to numerical simulations in the following.

4.2. Ray-tracing simulation

The first purpose of the simulations was therefore to validate the calculations made. For this reason, simulations were initially carried out by decoupling the contributions deriving from the source and from the analyzer. Figure 7a represents a simulation referred to the analyzer contribution while Figure 7b a simulation referred to the source contribution. Both simulated graphs show a perfect agreement with the respective probability densities predicted by the theory (Equations 3 and 5). The agreement between the analytical calculation above and the numerical simulations is extremely satisfactory and confirms our intellectual control on the geometric contributions to energy resolution of the spectrometer.

The overall geometric contribution to energy resolution is reported in Figure 8 for a Ge[220] Johansson ($R = 50\,\text{cm}$) crystal of 10×1 cm^2 and considering a source with FWHM along the two axes respectively equal to 35 µm and 300 µm. The Ge[440] and Ge[660] reflections can be directly deduced from Figure 8 multiplying respectively by 2 or 3 both axes:

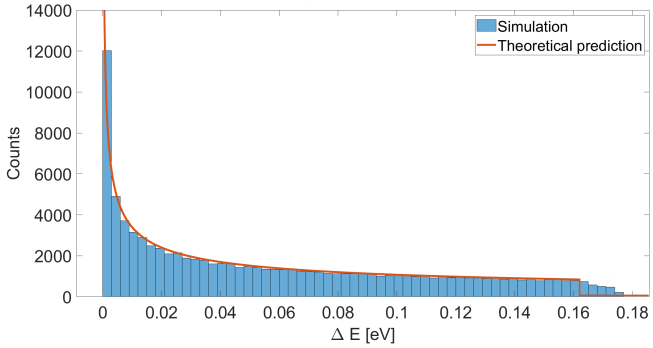

(a) Analyzer probability distribution p_a at $\theta_B = 75°$

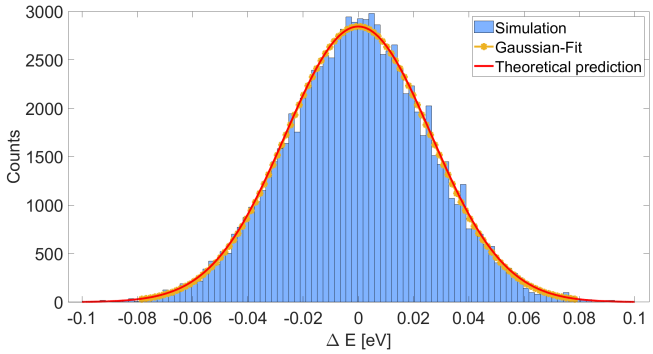

(b) Source probability distribution p_s at $\theta_B = 75°$

Figure 7: Frequency distributions simulated respectively with a point source and a 10×1 cm^2 analyzer and with a Gaussian source 35×300 µm^2 ($FWHM^2$) and a point-like analyzer. Ge[220] reflections are here considered.

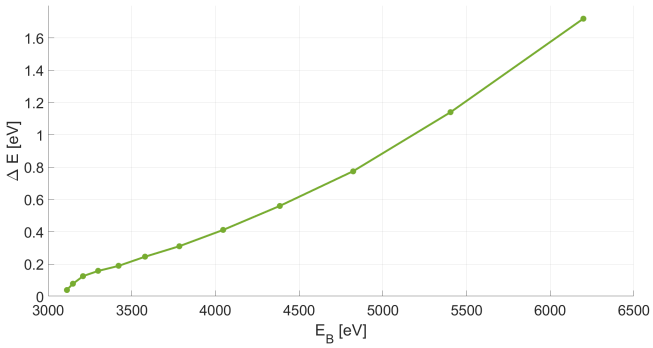

Figure 8: The FWHM of the total geometric contribution to energy resolution is here reported as a function of the Bragg energy E_B. The Ge[220] reflection for a Johansson ($R = 50\,\text{cm}$) crystal of 10×1 cm^2 surface and a Gaussian source of 35×300 µm^2 ($FWHM^2$) are considered.

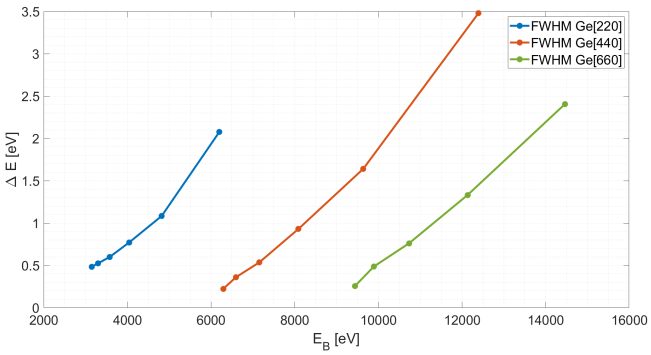

Figure 9: FWHM of the overall energy resolution of the spectrometer considering a Johansson ($R = 50\,\text{cm}$) crystal of 10×1 cm^2 surface and a source of 35×300 µm^2 ($FWHM^2$).

5. Overall energy resolution

Considering in addition the *intrinsic contribution to energy resolution* simulated through *tb-calc* software [5] it was thus possible to estimate the overall resolution of the spectrometer for the reflection Ge[220] and the following two harmonics (see Figure 9). Thanks to the partial overlap between different reflections we can cover the entire energy spectrum from $E_B = 3\,\text{keV}$ up to $E_B = 14\,\text{keV}$ keeping the overall energy resolution below 2 eV. The most critical point of the whole scan is paradoxically around $E_B = 6\,\text{keV}$ where we must reach $\theta_B = 29°$ in order to reach the overlap with the Ge[440] reflection at $\theta_B = 75°$.

6. Conclusions

We designed a user-friendly laboratory XAS spectrometer covering the $3 - 15$ keV energy range with an energy resolution below 3 eV aiming at limiting its costs and minimizing its dimensions. In order to achieve these challenging goals, an in-depth study was carried out on the shape of the crystals and on the geometric contribution to energy resolution. We selected a Johansson-type cylindrically bent analyzer with curvature radius $R = 50\,\text{cm}$ and dimensions 10×1 cm^2 exploiting also the reflections of the first and second harmonics of Ge[220]. The design will soon be completed and will be followed by the purchase of the necessary pieces and the subsequent construction of the instrument.

7. Acknowledgements

A special thanks goes to my advisors, Prof. Marco Moretti and Prof. Giacomo Ghiringhelli, and to all the doctoral students of the PoliMiX group. I would also like to underline the important work made by Matteo Corti and Andrea Cordone who accompanied me in this project giving an important contribution.

References

[1] Diego Gianolio. How to start an xas experiment. *X-Ray Absorption and X-Ray Emission Spectroscopy: Theory and Applications*, 1, 2016.

[2] M Moretti Sala, K Martel, C Henriquet, A Al Zein, L Simonelli, C Sahle, H Gonzalez, M-C Lagier, C Ponchut, S Huotari, et al. A high-energy-resolution resonant inelastic x-ray scattering spectrometer at id20 of the european synchrotron radiation facility. *Journal of synchrotron radiation*, 25(2):580–591, 2018.

[3] GT Seidler, DR Mortensen, AJ Remesnik, JI Pacold, NA Ball, N Barry, M Styczinski, and OR Hoidn. A laboratory-based hard x-ray monochromator for high-resolution x-ray emission spectroscopy and x-ray absorption near edge structure measurements. *Review of Scientific Instruments*, 85(11):113906, 2014.

[4] Mauro Rovezzi, Alistair Harris, Blanka Detlefs, Timothy Bohdan, Artem Svyazhin, Alessandro Santambrogio, David Degler, Rafal Baran, Benjamin Reynier, Pedro Noguera Crespo, et al. Texs: in-vacuum tender x-ray emission spectrometer with 11 johansson crystal analyzers. *Journal of synchrotron radiation*, 27(3):813–826, 2020.

[5] A-P Honkanen and Simo Huotari. General method to calculate the elastic deformation and x-ray diffraction properties of bent crystal wafers. *IUCrJ*, 8(1):102–115, 2021.